SECURITY CLASSIFICATION OF THIS PAGE

REPORT DOCUMENTATION PAGE

Form Approved
OMB No 0704-0188

1a REPORT SECURITY CLASSIFICATION
UNCLASSIFIED

1b RESTRICTIVE MARKINGS

2a SECURIT

2b DECLAS

3 DISTRIBUTION / AVAILABILITY OF REPORT
APPROVED FOR PUBLIC RELEASE;
DISTRIBUTION UNLIMITED

4 PERFORM **AD-A228 649**

5 MONITORING ORGANIZATION REPORT NUMBER(S)

6a NAME OF PERFORMING ORGANIZATION
MASSACHUSETTS INSTITUTE OF TECHNOLOGY

6b OFFICE SYMBOL (If applicable)

7a NAME OF MONITORING ORGANIZATION

6c ADDRESS (City, State, and ZIP Code)
EARTH, ATMOSPHERIC AND PLANETARY SCIENCES
77 MASSACHUSETTS AVE
CAMBRIDGE, MA 02139

7b ADDRESS (City, State, and ZIP Code)
OFFICE OF NAVAL RESEARCH RESIDENT REPN66017
MASSACHUSETTS INSTITUTE OF TECHNOLOGY
ROOM E19-628

8a NAME OF FUNDING / SPONSORING ORGANIZATION
OFFICE OF NAVAL RESEARCH

8b OFFICE SYMBOL (If applicable)

9 PROCUREMENT INSTRUMENT IDENTIFICATION NUMBER
N00014-89-J-3173

8c ADDRESS (City, State, and ZIP Code)
800 NORTH QUINCY STREET
ARLINGTON, VA 22217-5000

10 SOURCE OF FUNDING NUMBERS

PROGRAM ELEMENT NO	PROJECT NO	TASK NO	WORK UNIT ACCESSION NO

11 TITLE (Include Security Classification)
UNCLASSIFIED: Stochastic Modeling of Seafloor Morphology in Support of the Acoustic Reverberation SRP

12 PERSONAL AUTHOR(S)
JORDAN, THOMAS H. & GOFF, JOHN

13a TYPE OF REPORT	13b TIME COVERED	14 DATE OF REPORT (Year, Month, Day)	15 PAGE COUNT
FINAL REPORT	FROM 6/1/89 TO 12/31/89	1990 OCTOBER 29	24

16 SUPPLEMENTARY NOTATION

17 COSATI CODES		
FIELD	GROUP	SUB-GROUP

18 SUBJECT TERMS (Continue on reverse if necessary and identify by block number)
quantitative geomorphology, terrain analysis, reverberation acoustic scattering, mid-ocean ridge system, Sea Beam data

19 ABSTRACT (Continue on reverse if necessary and identify by block number)

This final technical report describes two numerical models of small scale seafloor topography, SM1-P, corresponding to a 100km x 100km area of the east central Pacific Ocean near the Cocos-Pacific spreading center of the east Pacific Rise, and SM1-A, corresponding to a 100km x 100km area of the North Atlantic Ocean west of the Mid-Atlantic Ridge. The models comprise both a deterministic component, taken from the DBDB5 digital bathymetric data base, and a stochastic component, obtained as a single realization of a five-parameter Gaussian random field describing the abyssal-hill topography. The parameters assumed in computing the stochastic realizations have been estimated from Sea Beam swaths passing through or near the study areas. SM1-P and SM1-A are specified by nested series of 1000x1000 point data files, which are available from the authors on 9-track magnetic tape. The nesting scheme employs a factor-of-ten reduction in scale on grids with knot spacings ranging from 100m to 0.1m.

20 DISTRIBUTION / AVAILABILITY OF ABSTRACT
☒ UNCLASSIFIED/UNLIMITED ☒ SAME AS RPT ☐ DTIC USERS

21 ABSTRACT SECURITY CLASSIFICATION
UNCLASSIFIED

22a NAME OF RESPONSIBLE INDIVIDUAL	22b TELEPHONE (Include Area Code)	22c OFFICE SYMBOL
Dr. Marshall Orr	703/696-4204	Code 11250A

DD Form 1473, JUN 86 Previous editions are obsolete SECURITY CLASSIFICATION OF THIS PAGE

S/N 0102-LF-014-6603

FINAL TECHNICAL REPORT

TO THE OFFICE OF NAVAL RESEARCH

PROJECT ON ACOUSTIC REVERBERATION

ONR CONTRACT N00014-89-J-3173

"Stochastic Modeling of Seafloor Morphology in Support of the Acoustic Reverberation SRP"

for the period
1 June 1989 - 31 December 1989

Principal Investigator:

Thomas H. Jordan
Head, Department of Earth,
Atmospheric and Planetary Sciences

Pacific and Atlantic Models of Small-Scale Seafloor Topography

JOHN A. GOFF AND THOMAS H. JORDAN

Department of Earth, Atmospheric and Planetary Sciences, Massachusetts Institute of Technology, Cambridge, MA 02139

SUMMARY

This final technical report describes two numerical models of small-scale seafloor topography, SM1-P, corresponding to a 100 km × 100 km area of the east central Pacific Ocean near the Cocos-Pacific spreading center of the East Pacific Rise and SM1-A, corresponding to a 100 km × 100 km area of the North Atlantic Ocean west of the Mid-Atlantic Ridge. The models comprise both a deterministic component, taken from the DBDB5 digital bathymetric data base, and a stochastic component, obtained as a single realization of a five-parameter Gaussian random field describing the abyssal-hill topography. The parameters assumed in computing the stochastic realizations have been estimated from Sea Beam swaths passing through or near the study areas. SM1-P and SM1-A are specified by a nested series of 1000 × 1000 point data files, which are available from the authors on 9-track magnetic tape. The nesting scheme employs a factor-of-ten reduction in scale on grids with knot spacings ranging from 100 m to 0.1 m.

Keywords: Numerical methods/procedures; Ocean bottom topography; Stochastic processes; Bathymetry; Geomorphology; Acoustic scattering; Ocean/terrain models; Random variables; Ocean ridges. (MM)

TABLE OF CONTENTS

1. INTRODUCTION

A principal scientific goal of the ONR Acoustic Reverberation SRP is to understand acoustic scattering from the deep-ocean bottom. A crucial component of this work is the development of realistic morphological models that can be used in numerical modeling of acoustic interactions with the seafloor. This report describes the first release of a set of models that will be generated for this purpose.

The models in this first release represent seafloor topography over a spectrum of horizontal scales ranging from 100 km to 0.1 m. The two areas selected for this study are a 100 km × 100 km region of the east central Pacific Ocean, near the Cocos-Pacific spreading center of the East Pacific Rise, and 100 km × 100 km area of the North Atlantic Ocean, west of the Mid-Atlantic Ridge. The numerical models of these regions, designated Seafloor Morphology 1-Pacific (SM1-P) and Seafloor Morphology 1-Atlantic (SM1-A), respectively, comprise both a deterministic component and a stochastic component. The deterministic component is taken from the DBDB5 digital bathymetric data base, which has a nominal horizontal resolution of 5' × 5'.

The stochastic component is obtained as a single (arbitrary) realization of the five-parameter Gaussian-random-field model developed by *Goff and Jordan* [1988, 1989*a*] to represent abyssal-hill topography. The parameters assumed in computing the stochastic realizations have been estimated by applying the inversion procedures of *Goff and Jordan* [1988] to Sea Beam swaths passing through or near the study areas. In Section 2, we review the stochastic model and describe some of its mathematical properties. Numerical tests of the inversion algorithm are discussed by *Goff and Jordan* [1989*b*], and comparisons between synthetic realizations of the Gaussian model and actual Sea Beam and SeaMARC II data sets are presented by *Goff and Jordan* [1988] and *Goff et al.* [1990]. The data-synthetic comparisons indicate that the model is generally successful at matching the low-order characteristics of abyssal hill terrain. Improvements in the model are anticipated, primarily through improved parameterizations of the two-point correlation function and the addition of higher-order terms in the stochastic characterization [*Goff and Jordan*, 1990]. However, it is hoped that the preliminary Gaussian models presented here will prove useful in testing numerical schemes for modeling acoustic reverberations generated by small-scale seafloor topography.

The complete representation of topography within a 10^4-km^2 area at the finest scale of resolution utilized our calculations, 0.1 m, requires the specification of 10^{12} grid points.

Data sets of this magnitude are too large to be feasibly handled with current computing technology. Therefore, the models are specified by a nested series of 1000×1000 point data files. The nesting scheme, described in Section 3, employs a factor-of-ten reduction in scale between each of four levels:

Level	Area (km × km)	Grid Spacing (m)
0	100×100	100
1	10×10	10
2	1×1	1
3	0.1×0.1	0.1

Data files containing the SM1-P and SM1-A models, together with software for manipulating these files, are available from the authors on 9-track magnetic tape. Technical information regarding the data structure and software is listed in Section 4.

2. DETERMINISTIC AND STOCHASTIC COMPONENTS OF SEAFLOOR TOPOGRAPHY

We let $z(\mathbf{x})$ be the height of the seafloor above some mean reference level at a position $\mathbf{x}$, and we suppose we have a map of this topography, denoted $z_M(\mathbf{x})$. Because the map is based on limited data, it may accurately represent age-dependent subsidence, thermal swells, major fracture zones, oceanic plateaus, and other "large-scale" features, but does not contain topographic variations with horizontal dimensions below some "cutoff scale" x_M. We assume the map can be approximated as the output of some filter $\mathcal{M}[z(\mathbf{x})]$. To the extent that the mapping cutoff is sharp — i.e., $\mathcal{M}$ passes features larger than x_M with no distortion but completely annihilates features smaller than x_M — this filter is a projection operator: $z_M(\mathbf{x}) = \mathcal{M}[z_M(\mathbf{x})]$. An example of $z_M(\mathbf{x})$, the one used in this report, is the DBDB5 bathymetry, which is specified on a $5' \times 5'$ grid (9.25-km knot spacing) and has an effective cutoff of $x_M \approx 50$ km.

We seek to supplement this deterministic description of the seafloor with some stochastic representation of the small-scale features. Let $h(\mathbf{x})$ be a stochastic process, or random field, which represents the statistics of the topographic variation at all length scales. We define $h_M(\mathbf{x}) = \mathcal{M}[h(\mathbf{x})]$ and take as our model of seafloor topography

$$\tilde{z}(\mathbf{x}) = z_M(\mathbf{x}) + h(\mathbf{x}) - h_M(\mathbf{x}) \quad (1)$$

In other words, we replace the stochastic components of the field with scale lengths greater than the cutoff x_M by the known ("deterministic") components. If $\mathcal{M}$ is a projection operator, then applying it to this model recovers the map: $\mathcal{M}[\tilde{z}(\mathbf{x})] = z_M(\mathbf{x})$.

3. Gaussian Model of Small-Scale Topography

The stochastic model used in this report is a stationary (spatially homogeneous) Gaussian random field with zero mean and a 2-point moment (covariance) function,

$$C_{hh}(\mathbf{x}) = \langle h(\mathbf{x}_1)\, h(\mathbf{x}_1 + \mathbf{x}) \rangle \quad (2)$$

where $\langle \cdot \rangle$ is the expected value and $\mathbf{x}$ is the lag vector. Under the Gaussian assumption, all higher moments of the random field can be expressed in terms of (2). The power spectrum of the Gaussian field is the Fourier transform of this covariance function [*Bracewell*, 1978], and its phase spectrum is a random process uniformly distributed on $(0,2\pi]$ [*Priestly*, 1981].

Although the distribution of seafloor depths often fails the Kolmogorov-Smirnov test for acceptance of the Gaussian hypothesis [*Gilbert and Malinverno*, 1988], approximating small-scale topography by a Gaussian field provides a simple and mathematically convenient description of its most important features [*Bell*, 1975; *Goff and Jordan*, 1988]. These include its RMS height variation, the orientation and characteristic wavenumbers of its "tectonic grain," and the variation of roughness with spatial scale. Moreover, a Gaussian description is the basis for the study of higher-order statistical properties, which can be expressed as perturbations from a Gaussian form [*Goff and Jordan*, 1990].

Covariance model. The mathematical properties of the two-dimensional Gaussian process employed in this study are detailed in *Goff and Jordan* [1988, 1989*a*]. To represent small-scale abyssal-hill topography, we have proposed a covariance function of the form

$$C_{hh}(\mathbf{x}) = H^2\, G_\nu(r(\mathbf{x})) \,/\, G_\nu(0) \quad (3)$$

where H is the RMS height and G_ν is defined by

$$G_\nu(r) = r^\nu K_\nu(r), \quad 0 \le r < \infty, \quad \nu \in [0,1] \tag{4}$$

K_ν is the modified Bessel function of the second kind of order ν. G_ν is plotted for three values of ν in Figure 1 (top panel). The order parameter ν controls the behavior of $G_\nu(r)$ at the origin; its slope at $r = 0$ is zero for $\nu = 1$ and infinite for $\nu = 0$. $G_{1/2}(r)$ is simply an exponential function.

Azimuthal variation is expressed by the dimensionless ellipsoidal (Riemannian) norm

$$r(\mathbf{x}) = \left[\mathbf{x}^T \mathbf{Q}\, \mathbf{x} \right]^{1/2} = \sqrt{q_{11}x_1^2 + 2q_{12}x_1x_2 + q_{22}x_2^2} \tag{5}$$

The scale matrix, $\mathbf{Q}$, can be expressed in terms of its ordered eigenvalues $k_n^2 \ge k_s^2$ and its normalized eigenvectors $\hat{\mathbf{e}}_n$ and $\hat{\mathbf{e}}_s$,

$$\mathbf{Q} = k_n^2 \hat{\mathbf{e}}_n \hat{\mathbf{e}}_n^T + k_s^2 \hat{\mathbf{e}}_s \hat{\mathbf{e}}_s^T \tag{6}$$

$\mathbf{Q}$ specifies the "outer scale" of the topography through the characteristic wavenumbers k_n and k_s, yielding an aspect ratio $a = k_n/k_s$ for the lineation or "tectonic grain" of the abyssal hills. The orientation of this anisotropy is given by the directions of the principal axes. Since the covariance decays least rapidly along the $\hat{\mathbf{e}}_s$ axis, the structure tends to be lineated in this direction.

Thus, five parameters determine the stochastic model: the RMS height H, the order parameter ν, the characteristic wavenumbers k_n and k_s, and the azimuth ζ_s of $\hat{\mathbf{e}}_s$ in the geographic reference frame. The scale parameters define an aspect ratio $a = k_n/k_s$.

Power spectrum. The power spectrum obtained from Fourier transforming (3) is

$$P_h(\mathbf{k}) = 4\nu\pi H^2 |\mathbf{Q}|^{1/2} \left[u(\mathbf{k}) + 1\right]^{-(\nu+1)} \tag{7}$$

where u is the dimensionless norm of $\mathbf{k}$ defined in terms of its modulus k and azimuth ζ by

$$u(\mathbf{x}) = \left[\mathbf{k}^T \mathbf{Q}^{-1} \mathbf{k} \right]^{1/2} = \sqrt{(k/k_s)^2 \cos^2(\zeta-\zeta_s) + (k/k_n)^2 \sin^2(\zeta-\zeta_s)} \tag{8}$$

The one-dimensional forms of the power spectrum at three values of ν are shown in Figure 1 (bottom panel). Equation (7) is a power-law spectrum with a corner wavenumber k_n in

the $\hat{\mathbf{e}}_n$ direction and k_s in the $\hat{\mathbf{e}}_s$ direction. At high wavenumbers the power spectrum decays at a rate $k^{-(\nu+1)}$; at low wavenumbers, it is flat.

Hausdorff dimension and self-affine scaling. The Hausdorff (fractal) dimension D of a topographic surface can be related to the asymptotic properties of the covariance function at small lag [*Adler*, 1981]. *Goff and Jordan* [1988] show that the Hausdorff dimension associated with (3) is

$$\mathsf{D} = 3 - \nu \tag{9}$$

Decreasing the parameter ν increases the roughness, with the limiting cases of unity and zero corresponding to a Euclidean random field with continuous derivative (D = 2) and one which is "space-filling" (D = 3), respectively.

The Hausdorff dimension describes a self-affine scaling relationship at wavenumbers much larger than k_n [*Goff and Jordan*, 1988, 1989*a*]. A topographic surface $h(\mathbf{x})$ is self-affine if there exists an $\alpha \in [0,1]$ such that, for all $R > 0$ the topographic difference function $d(\mathbf{x} - \mathbf{x}_0) = h(\mathbf{x}) - h(\mathbf{x}_0)$ is identical in distribution to $R^{-\alpha} d(R\mathbf{x} - R\mathbf{x}_0)$. For the covariance model (3), *Goff and Jordan* [1988] demonstrate that $\alpha = \nu$. The self-affine property allows the topography at high wavenumber to be simply interpolated to smaller scales. However, the validity of this interpolation at scales below the resolution of bathymetric mapping devices is hypothetical; some work suggests that the spectral exponent [*Fox and Hayes*, 1985] and aspect ratio [*Goff and Jordan*, 1990] are scale-variable. Small-scale stochastic interpolation using the covariance model (3), including the high-resolution synthetic realizations accompanying this technical report, require testing in the natural-laboratory settings that will be investigated during the SRP.

Characteristic scales. Unlike spectral models usually associated with fractals [e.g. *Mandelbrot*, 1983], a random field whose second-order properties are described by (3) or (7) does not have infinite power at zero wavenumber. Rather, the low-wavenumber part of the spectrum is governed by a characteristic length, or outer scale. As discussed in *Goff and Jordan* [1988], the characteristic length in the θ direction, λ_θ, can be defined in terms of the second moment of the covariance function in the θ direction, which yields

$$\lambda_\theta = \frac{2\sqrt{2(\nu + 1/2)}}{k_\theta}, \quad k_\theta = \left[\hat{\mathbf{e}}_\theta^{\mathsf{T}} \mathbf{Q} \, \hat{\mathbf{e}}_\theta^{\mathsf{T}} \right]^{1/2} \tag{10}$$

where k_θ is the scale parameter in the θ direction. λ_n is interpreted as the characteristic abyssal-hill width, and λ_s as the characteristic abyssal-hill length.

Slope statistics. The characterization of topographic slopes is critical to modeling acoustic reverberation, and it has important geological applications [e.g., *Smith and Shaw*, 1989]. We therefore give some simple mathematical properties of the slope distributions derived from our Gaussian model. Because the covariance function (3) is discontinuous at the origin for $\nu < 1$, the random field has fractal character, and its spatial derivatives do not exist. Therefore, it is necessary to measure slopes in terms of topography differences over finite intervals. The slope function is defined as

$$s(\mathbf{x}_1,\xi_1) = \frac{h(\mathbf{x}_1 + \xi_1) - h(\mathbf{x}_1)}{|\xi_1|} \tag{11}$$

where $|\xi_1|$ is the slope interval. If the probability density function for h is stationary and normally distributed with known second moment, as in (3), then the probability density function for s will also be stationary and normally distributed with zero mean and variance given by

$$\langle s^2(\mathbf{x}_1,\xi_1)\rangle = \frac{2(C_{hh}(0) - C_{hh}(\xi_1))}{|\xi_1|^2} \tag{12}$$

We can also calculate the slope autocovariance:

$$C_{ss}(\mathbf{x},\xi_1,\xi) = \langle s(\mathbf{x}_1,\xi_1)\, s(\mathbf{x}_1 + \mathbf{x},\xi_1 + \xi)\rangle = \frac{C_{hh}(\mathbf{x} + \xi) - C_{hh}(\xi_1 - \mathbf{x}) - C_{hh}(\mathbf{x} + \xi_1 + \xi) + C_{hh}(\mathbf{x})}{|\xi_1|\,|\xi_1 + \xi|} \tag{13}$$

and the slope-height covariance

$$C_{sh}(\xi_1) = \frac{C_{hh}(\xi_1) - C_{hh}(0)}{|\xi_1|} \tag{14}$$

In one dimension, the case $\nu = 0.5$ (exponential covariance) yields a Markov process (the Ornstein-Uhlenbeck process) [*Feller*, 1971]. The Markov property can be demonstrated by considering the 1-D form of (13) for $k_\theta \xi \ll 1$:

$$C_{ss}(x,\xi_1,\xi) = \begin{cases} \dfrac{2H^2 k_\theta}{|\xi_1|} \dfrac{(\xi_1 - x)}{(\xi_1 + \xi)}, & \xi_1 > x \\ 0, & \xi_1 \le x \end{cases} \tag{15}$$

Thus, when slope intervals do not overlap ($\xi_1 < x$), the slopes are uncorrelated.

Nearby slopes are positively correlated where $\nu > 0.5$, and negatively correlated where $\nu < 0.5$.

4. ALGORITHM FOR GENERATING SYNTHETIC TOPOGRAPHY ON NESTED GRIDS

The algorithm for generating nested synthetics involves two basic steps. The first is to generate a master realization from the desired covariance function on a large-scale grid (here, 100 km × 100 km). The second is to take a compact rectangular subset of the master realization and use it as a constraint in generating a synthetic realization with finer resolution. The latter involves a procedure for "molding" an arbitrary topographic array to values specified on a coarser grid. The nested synthetic is then regarded as a master realization, and the nesting is iterated to produce realizations on finer grids.

To generate the 100 km × 100 km master realization, we compute the Fourier spectrum on a regularly spaced wavenumber grid by multiplying the square root of the power spectrum (7) by a phase factor $\exp(i\phi)$, where ϕ is a random number uniformly distributed on the interval $[0, 2\pi)$ [*Priestly*, 1981]. The space domain image is then obtained from a two-dimensional, fast Fourier transform. (In all transforms, edge effects associated with aliasing are minimized by computing the realization on a grid 20% larger than required and stripping off the edges.) An example of such a realization, displayed as a color-contoured, grey-shaded relief plot, is shown in the upper left panel of Figure 2.

The algorithm for generating a nested synthetic realization includes the following steps:

1. A rectangular ($m \times n$ array) compact subset of the master realization is selected for nesting. As an example, we employ the 10 km × 10 km square outlined in white in the first panel of Figure 2. For this subset, $m = n = 100$.

2. The subset is interpolated using a bilinear (or bicubic) algorithm [*Press et. al.*, 1986] at the resolution that will be required for stochastic interpolation. This results in an $em \times en$ array, where e is the densification factor. The second panel of Figure 2 shows the bilinear interpolation of the box shown in the first panel with $e = 10$, which results in another 1000 × 1000 array.

3. A stochastic realization is generated from the covariance model at the resolution and scale required for the stochastic interpolation. The bilinear interpolation of the subset is Fourier transformed, obtaining a spectrum with discrete wavenumbers (k_{x_i}, k_{y_j}) indexed $-em/2 < i < em/2$ and $-en/2 < j < en/2$. Phases of the wavenumbers indexed $-m/2 < i < m/2$ and $-n/2 < j < n/2$, the portion of the spectrum sampled by the master realization, are then input as the phases for the identically indexed wavenumbers of the spectrum of the stochastic realization. The Fourier transform of this spectrum produces a realization whose low wavenumber characteristics are similar to those of the interpolated subset (compare the second and third panels of Figure 2).

4. The final step involves molding the finer-scale realization generated in step 3 to the master realization generated in step 1. The former is first sampled on the coarse grid, resulting in an $m \times n$ array. This array is then interpolated using the same algorithm used in step 2, yielding a second $em \times en$ array. The difference between this interpolated array and that obtained in step 2 is subtracted from the finer-scale realization, thus constraining it to coincide with the master on the coarser grid. The fourth panel in Figure 2 shows the final product.

The effect of the molding algorithm is to replace the smoother features of the unconstrained stochastic realization with those obtained from the master without significantly altering the power spectrum.

4. TECHNICAL SPECIFICATIONS FOR MODELS SM1-P AND SM1-A

Stochastic model. The following model parameters were used to generate the two series of stochastic realizations:

Model	H (m)	ζ_s (deg)	λ_n (km)	λ_s (km)	D
SM1-P	50	170	2.3	19	2.5
SM1-A	225	10	5.9	22	2.2

These parameters are derived from the inversion of Sea Beam swaths using the technique of *Goff and Jordan* [1988]. Model SM1-P was obtained from Sea Beam data taken near the East Pacific Rise between the Orozco and Siquieros fracture zones (see *Goff et al.* [1990]), and the Atlantic series from Sea Beam data taken just south of the Kane fracture zone.

Two sets of DBDB5 bathymetry, gridded at 10 km spacing and covering 100 km on a side, are also provided in the release. The Pacific data file is called PDBDB5, and the Atlantic data file ADBDB5. The FORTRAN code also provided in the release, merge.f, uses the molding algorithm to conform the largest scale synthetic realizations to the constraints of the DBDB5 sections. The two DBDB5 data sets and the superposition of these data sets with the (molded) stochastic realizations are shown in Figure 3.

Nesting geometry. The nesting geometry is shown in Figure 4. The first master realization array contains 1000 × 1000 points covering an area of 100 km × 100 km. Five subsets whose lower-left corner coordinates are shown in Figure 4, each a 100 × 100 array, are chosen for nesting. The densification factor is $e = 10$ so that the nested realizations will be 1000 × 1000 arrays covering 10 km on each side. The center nested realization is then chosen as the master realization for the next round of nesting. This procedure is iterated 3 times, yielding one master realization with 100-km sides (100-m grid spacing), 5 realizations with 10-km sides (10-m grid spacing), 5 realizations with 1-km sides (1-m grid spacing) and 5 realizations with 100-m sides (0.1-m grid spacing).

The realizations are designated by their locations (A = Atlantic, P = Pacific), iteration level (0-3), and subset number (1-5). The convention for naming the realizations are shown in Figure 4. P01 is the master realization for the Pacific series (SM1-P). The first set of nested realizations in this series are P11, P12, P13, P14, and P15. P11 is then chosen as the master realization with nested realizations P21 through P25. And finally (though not shown in Figure 4) P21 is used to generate realizations P31 through P35.

Figures 5 and 6 show the master realization and the five nested realizations of the first iteration level for SM1-P and SM1-A, respectively. The box outlines in the master realization (middle-top panel) are the subsets chosen for nesting. Figure 4 can be used to match the appropriate subset to the surrounding nested realizations.

Figures 7 and 8 show the number 1 subset of each iteration of the SM1-P and SM1-A, respectively. The character of the largest scale plots (P01 and A01) are dominated by the scale lengths λ_n and λ_s, i.e. by the abyssal hills. The range of scales exhibited by these plots lie predominantly within the white portion of the spectrum. Features with scale lengths larger than the characteristic length are not significantly greater in amplitude and so do not stand out. The range of scales in P11 and A11 are an order of magnitude smaller than those in P01 and A01, and they lie close to the corner region of the spectrum. While the characteristic length scales, on the order of the size of the plot, are still apparent, we also notice the rich texture at smaller scales. The scales represented in P21 and P31 (Figure 7), and A21 and A31 (Figure 8), are much smaller than the characteristic lengths; i.e., they contain features described by the sloping (fractal) portion of the power spectrum. The color scale and vertical exaggeration (which controls shading) have both been rescaled according to the self-affine scaling relationship discussed in Section 2. We therefore expect that the P21 and A21 plots and the P31 and A31 plots should be statistically similar. Visual inspection confirms this.

Aliasing. If the spectrum of a spatially unlimited topographic field $h(\mathbf{x})$ is sampled on and $N \times N$ grid of spacing Δk, its space-domain image will be an aliased version of $h(\mathbf{x})$. The covariance function of the aliased field will be the sum of the covariance function $C_{hh}(\mathbf{x})$ with copies centered on a grid with spacing $N\Delta x$ [*Bracewell*, 1978]. When $N\,\Delta x$ is large compared to the characteristic length λ_s, such as in the case of the master realization of each series, aliasing will not be significant, since the amplitude of the copies is small where $C_{hh}(\mathbf{x})$ is large. However, when $N\Delta x$ is small compared to the characteristic length, such as in the second-level and third-level nestings of each series, the spacing between copies is small enough that the aliased covariance function will be significantly different from the model.

Fortunately, the effect of aliasing is to add power to the field only at the largest scales. The combined contribution of nearby diametrically placed copies will be approximately a constant. Adding a constant to the covariance simply adds a constant to the topography, which is removed in the molding procedure.

File structure. Each synthetic realization is a written in a UNIX direct access FORTRAN binary data file with a record length of 4 bytes. Each record is a single REAL*4 number stored in IEEE format. The first eight numbers constitute the header. These numbers contain the following information:

1. Minimum x value of the realization array (consistent with the coordinates of the largest master array realization).
2. Maximum x value.
3. Minimum y value.
4. Maximum y value.
5. Number of elements in the x direction.
6. Number of elements in the y direction.
7. First four digits of the seed number used to initialize the pseudo-random number generator used to compute the phase values.
8. Last four digits of the seed number.

Following the header the realization values are given. The realization arrays are stored in columns (y values; i.e. where (i,j) is the indexing of the (x_i,y_j) coordinates, the first 1000 numbers are $(i = 1, j = 1)$ through $(i = 1, j = 1000)$, the second 1000 are $(i = 2, j = 1)$ through $(i = 2, j = 1000)$, etc.

The gridded DBDB5 files are written in ASCII, but are otherwise identical in file structure to the realization files, with the one exception that the 7th and 8th header values contain the latitude and longitude of the lower-left corner of the data set.

File storage. All files are written on a 6250 bpi 9-track tape using the UNIX tar utility. There are 16 files in each series. Each file is approximately 4 Mb in size. The total data size is approximately 128 Mb. Also included are the ASCII DBDB5 data sets and the FORTRAN program and subroutines for reading the files and for nesting one topographic array into a coarser array.

6. REFERENCES

Adler, R. J., *The Geometry of Random Fields*, 280 pp., John Wiley, New York, 1981.

Bell, T. H., Statistical features of sea-floor topography, *Deep Sea Res.*, **22**, 883-892, 1975.

Bracewell, R., *The Fourier Transform and its Applications*, 381 pp., McGraw-Hill, New York, 1978.

Feller, W., *An Introduction to Probability Theory and Its Applications, Vol. 2*, 669 pp., John Wiley, New York, 1971.

Fox, C. G., and D. E. Hayes, Quantitative methods for analyzing the roughness of the seafloor, *Rev. Geophys.*, **23**, 1-48, 1985.

Gilbert, L. E., and A. Malinverno, A characterization of the spectral density of residual ocean floor topography, *Geophys. Res. Lett.*, **15**, 1401-1404, 1988.

Goff, J. A., and T. H. Jordan, Stochastic modeling of seafloor morphology: inversion of Sea Beam data for second-order statistics, *J. Geophys. Res.*, **93**, 13589-13609, 1988.

Goff, J. A., and T. H. Jordan, Stochastic modeling of seafloor morphology: a parameterized Gaussian model, *Geophys. Res. Lett.*, **16**, 45-48, 1989a.

Goff, J. A., and T. H. Jordan, Stochastic modeling of seafloor morphology: resolution of topographic parameters by Sea Beam data, *IEEE J. Oceanic Eng*, **14**, 326-337, 1989b.

Goff, J. A., and T. H. Jordan, The use of the 3-point correlation function in the characterization of abyssal hill asymmetries (abstract), *Eos*, **70**, 1306, 1990.

Goff, J. A, T. H. Jordan, M. H. Edwards, and D. J. Fornari, Comparison of a stochastic seafloor model with SeaMARC II bathymetry and Sea Beam data near the East Pacific Rise 13° - 15° N, submitted to *J. Geophys. Res.*, 1990.

Mandelbrot, B. B., *The Fractal Geometry of Nature*, 468 pp., W. H. Freeman, New York, 1983.

Press, W. H., B. P. Flannery, S. A. Teukolsky, and W. T. Vetterling, *Numerical Recipes*, 818 pp., Cambridge, New York, 1986.

Priestly, M. B., *Spectral Analysis and Time Series*, 890 pp., Academic, San Diego, 1981.

Smith, D. K., and P. R. Shaw, Topographic patterns and slope distributions (abstract), *Eos*, **70**, 467, 1989.

7. FIGURES

Figure 1. Functional form of the model covariance function $G_\nu(r)$, plotted for values of $\nu = 0$, 1/2, and 1 (top panel), and their normalized Fourier transforms plotted on a log-log scale (bottom panel).

Figure 2. Example of the nesting algorithm described in Section 3 of the text. Each panel is a color-contoured, grey-shaded relief plot of seafloor topography. First panel (upper left) is the unconstrained master realization, generated from the parameters for SM1-P. This realization array contains 1000 × 1000 elements, and is 100 km on each side. The outlined box in the middle of this panel is the subset chosen for nesting. This box is 100 × 100 elements (10 km × 10 km). The second panel (upper right) is the bilinear interpolation of the subset. This panel contains 1000 × 1000 elements and has a dimension of 10 km × 10 km. The third panel (bottom left) is another stochastic realization generated over the finer-scale grid of the second panel. The phases from the lowest 50 wavenumbers from the Fourier spectrum of the second panel were used as phases for the identical wavenumbers in generating the third panel. The fourth panel (lower right) was then generated by molding (see text) the second panel to the constraints provided by the master.

Figure 3. Color-contoured, grey-shaded plots of the Pacific and Atlantic DBDB5 sections provided in the release and the superposition of these data sets with the (molded) stochastic realizations (see text). These topographic models are designated SM1-P and SM1-A, respectively Latitude and longitudes represent the location of the lower-left corner of each DBDB5 section.

Figure 4. Nesting geometry and file naming conventions for the SM1-P series. The files are named by their location (in this example, P = Pacific), their iteration number (0, 1, 2, or 3), and their subset number (1, 2, 3, 4, and 5). The master realization for the SM1-P is P01. It is a 1000 × 1000 array with 100-km sides. Five subset arrays, with lower-left coordinates shown, 100 × 100 elements, and 10 km sides, are chosen for nested realizations P11 through P15. The densification factor e equals 10, so that nesting generates 1000 × 1000 arrays with 10-km sides. The center nested realization, P11 is chosen as the next master realization and the process is iterated to produce nested realizations P21 through P25. In the last step, P21 is used to generate P31 through P35.

Figure 5. Color-contoured, grey-shaded plots of the master synthetic realization and nested realizations of the first iteration level for the Pacific series. Figure 4 matches subset boxes in the master realization (P01) with the nested realizations (P11 through P15).

Figure 6. Color-contoured, grey-shaded plots of the master synthetic realization and nested realizations of the first iteration level for the Atlantic series. Figure 4 matches subset boxes in the master realization (A01) with the nested realizations (A11 through A15).

Figure 7. Color-contoured, grey-shaded plots of the nested realizations of the first subset of each iteration of the SM1-P (Pacific) series. Box outline in the center of each plot represents the subset chosen for nesting at the next iteration level (see Figure 4). Color scale and vertical exaggeration of the P21 and P31 plot have been reset according to the self-affine relationship discussed in Section 2.

Figure 8. Color-contoured, grey-shaded plots of the nested realizations of the first subset of each iteration of the SM1-A (Atlantic) series. Box outline in the center of each plot represents the subset chosen for nesting at the next iteration level (see Figure 4). Color scale and vertical exaggeration (controling shading) of the A21 and A31 plot reset according to the self-affine relationship discussed in Section 2.

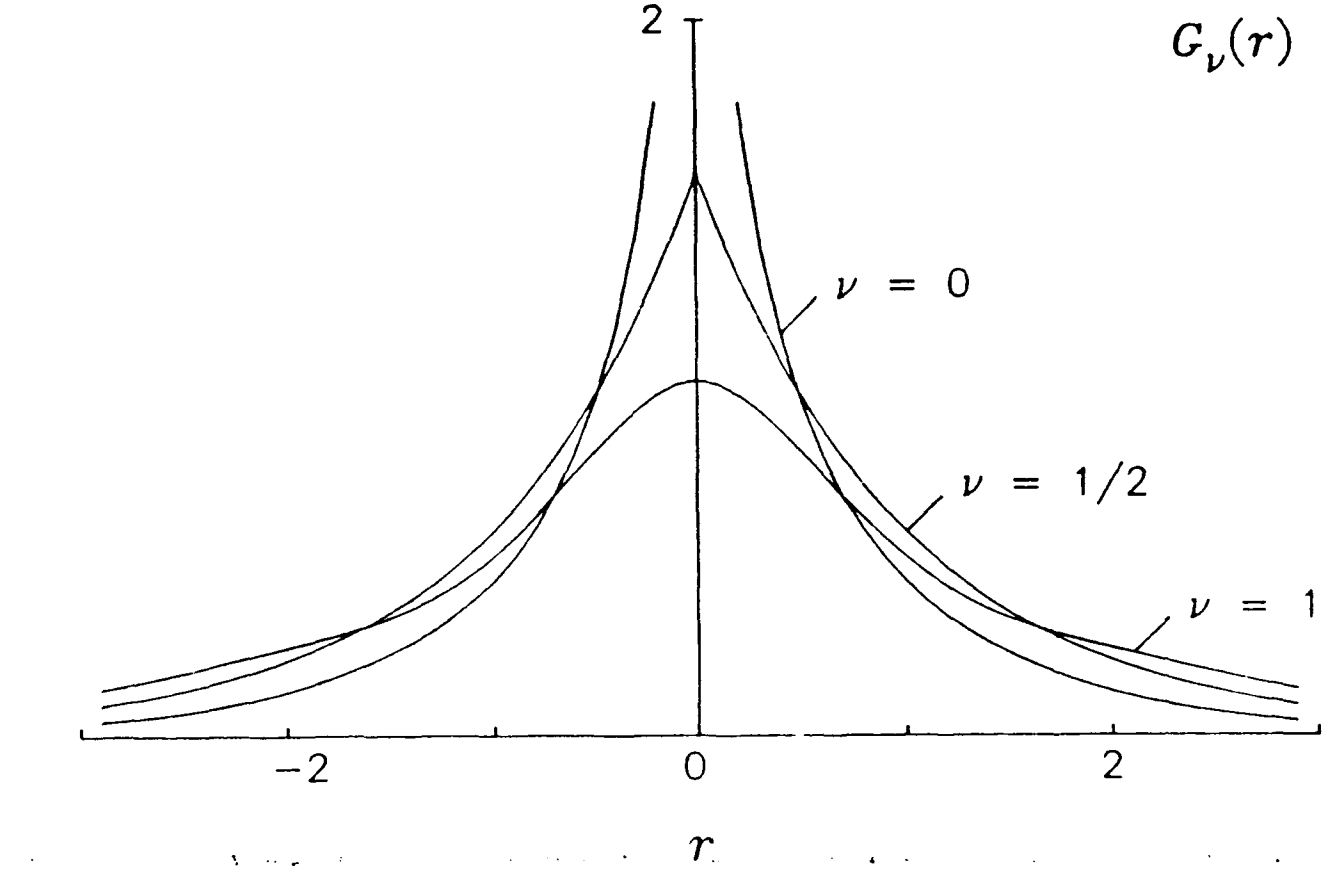

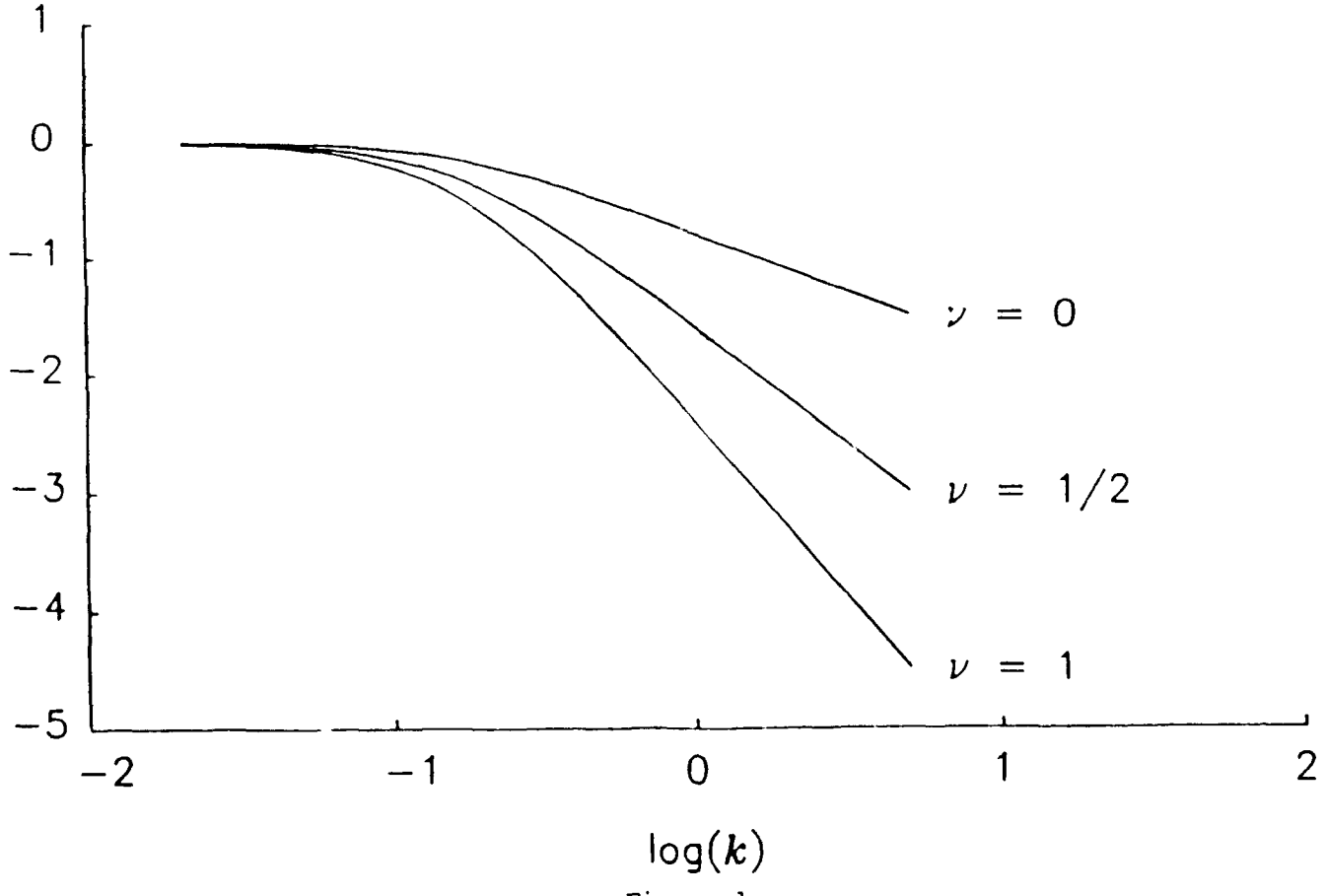

Figure 1

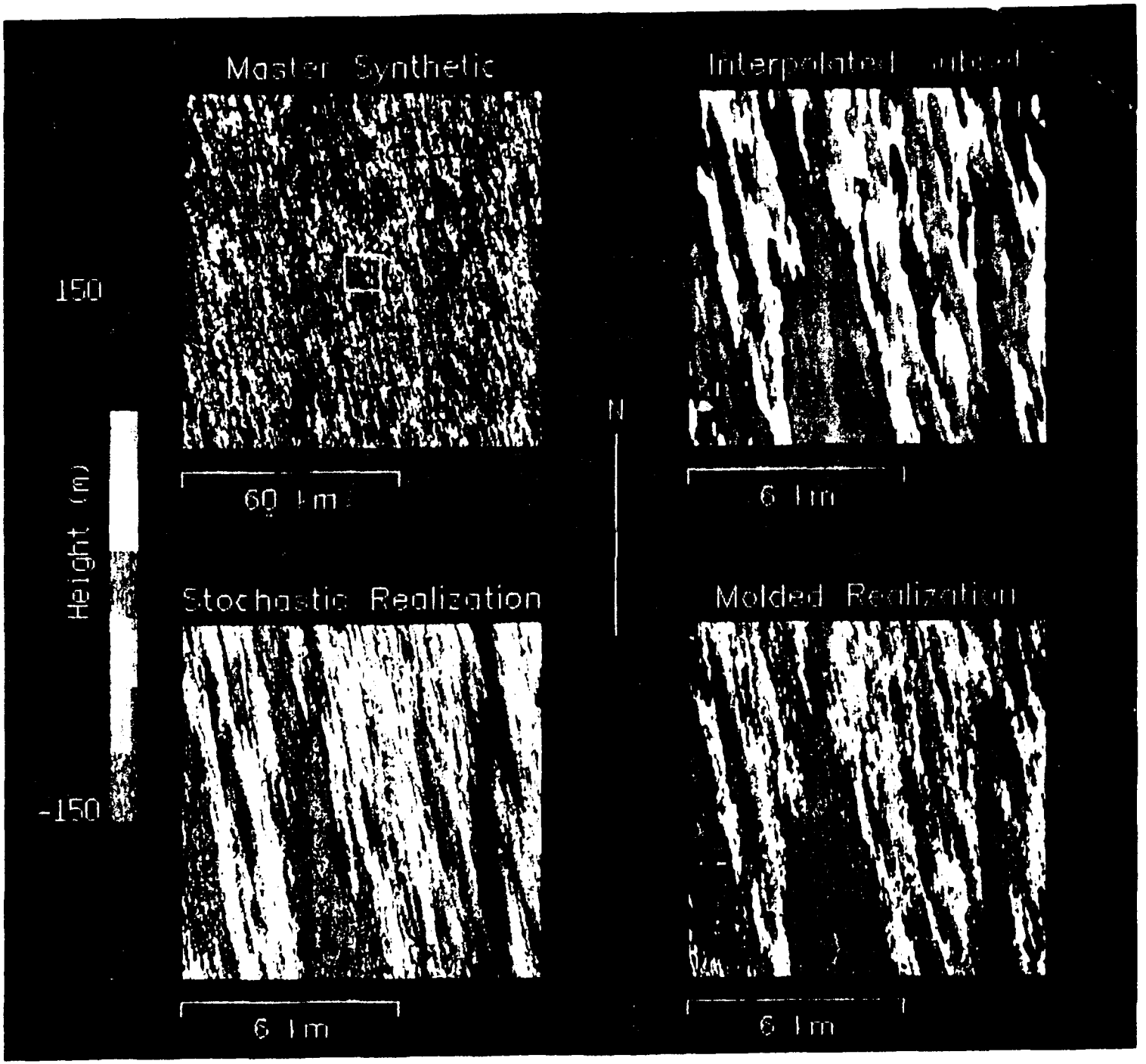
Master Synthetic
Interpolated
150
-150
Height (m)
N
60 1m
6 1m
Stochastic Realization
Molded Realization
6 1m
6 1m

Figure 2

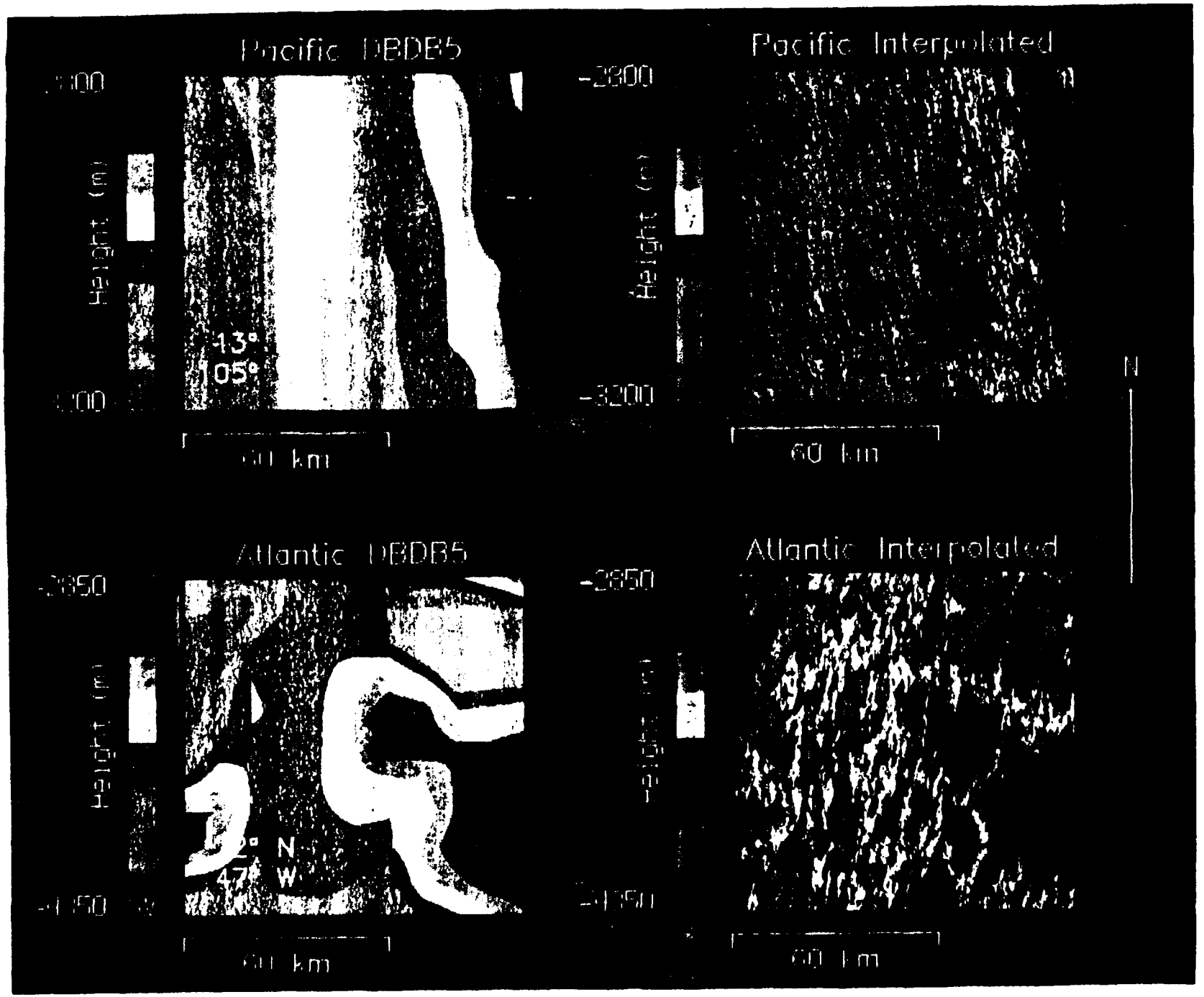
Pacific DBDB5
-2800
Height (m)
-3200
13°
105°
60 km
Pacific Interpolated
-2800
-3200
60 km
N
Atlantic DBDB5
-2850
Height (m)
-3250
2° N
47° W
60 km
Atlantic Interpolated
-2850
-3250
60 km

Figure 3

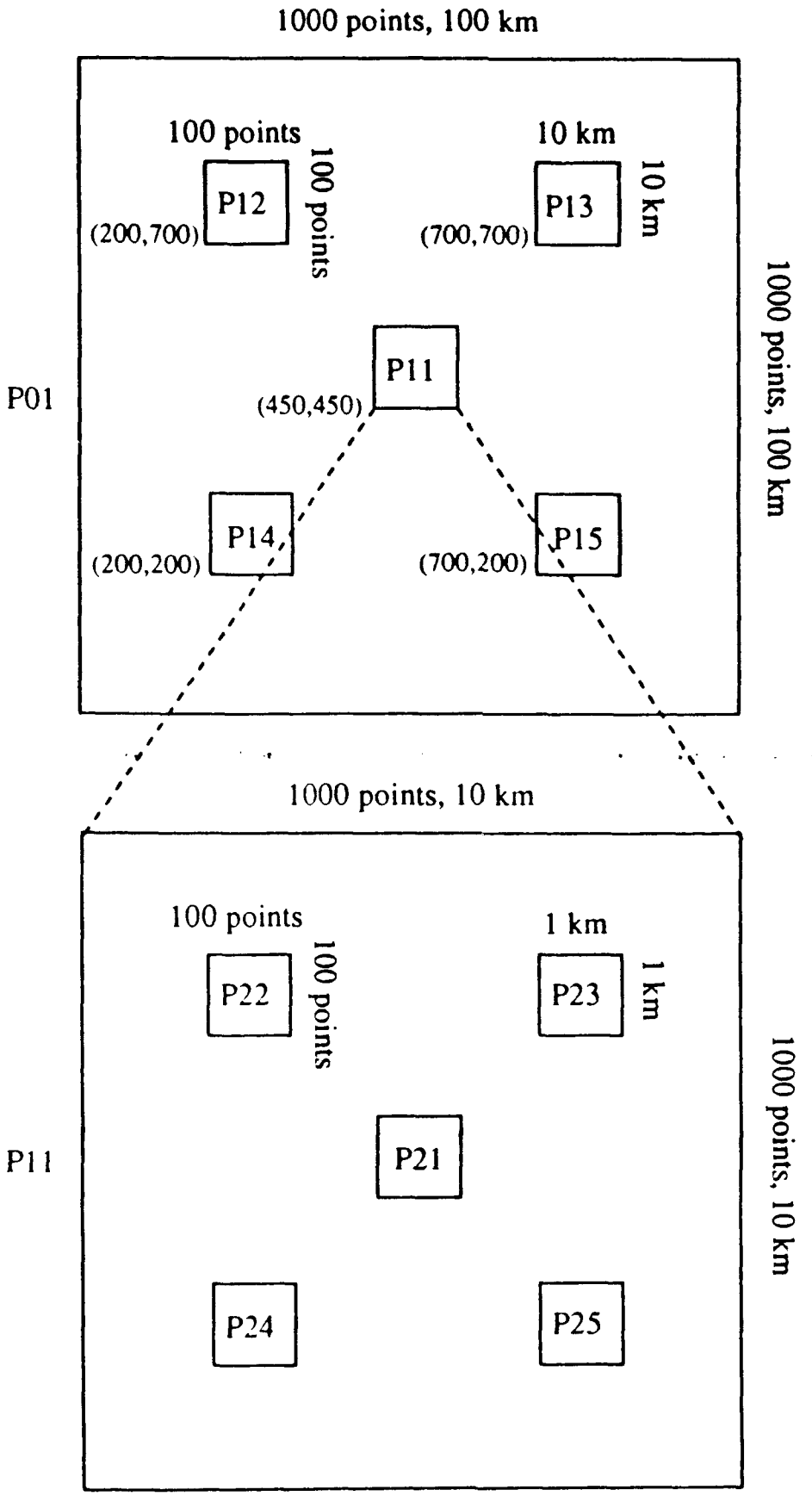
1000 points, 100 km
100 points
100 points
10 km
10 km
P12
(200,700)
P13
(700,700)
P11
(450,450)
P01
P14
(200,200)
P15
(700,200)
1000 points, 100 km
1000 points, 10 km
100 points
100 points
1 km
1 km
P22
P23
P21
P11
P24
P25
1000 points, 10 km

Figure 4

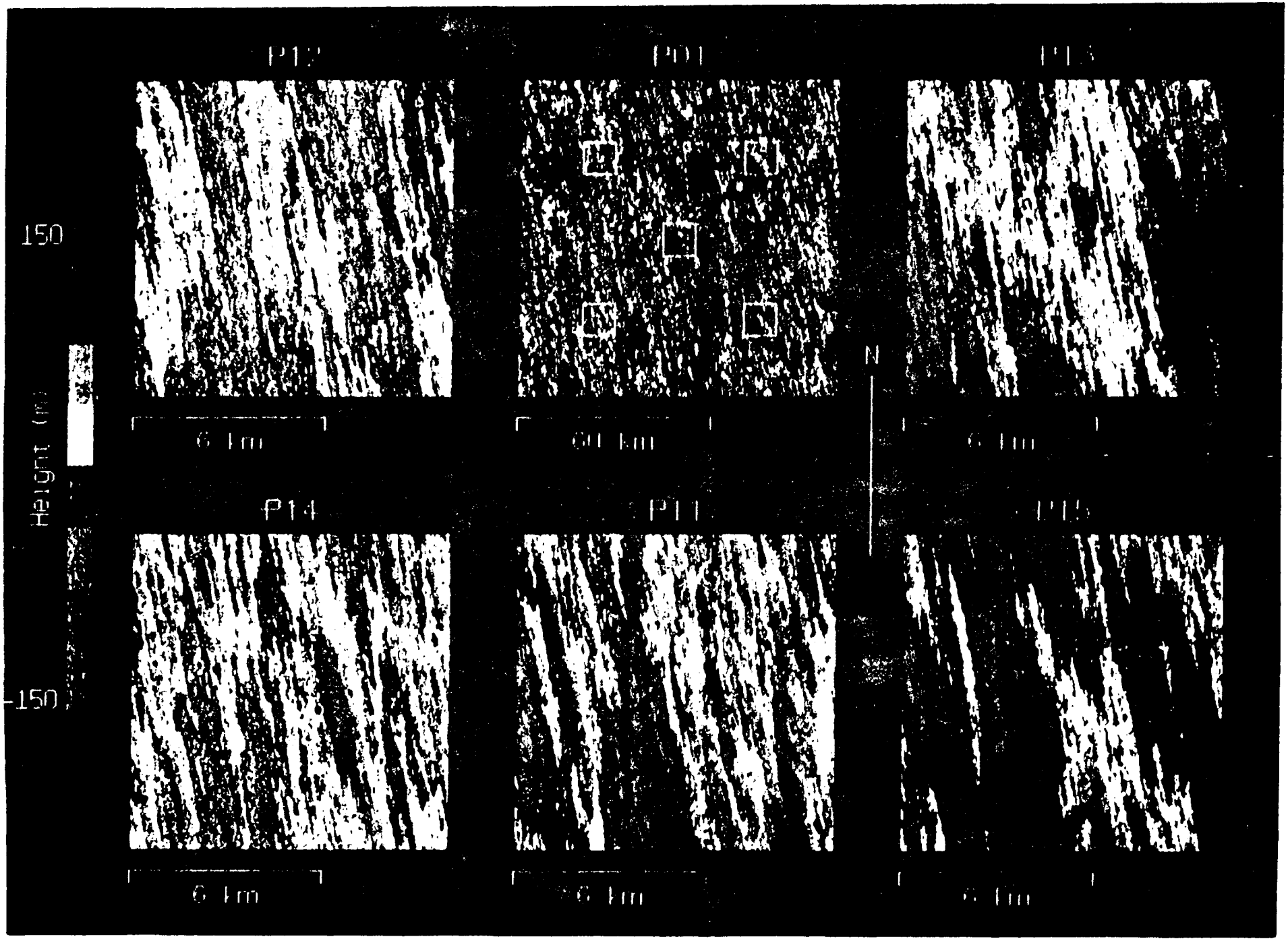

Figure 5

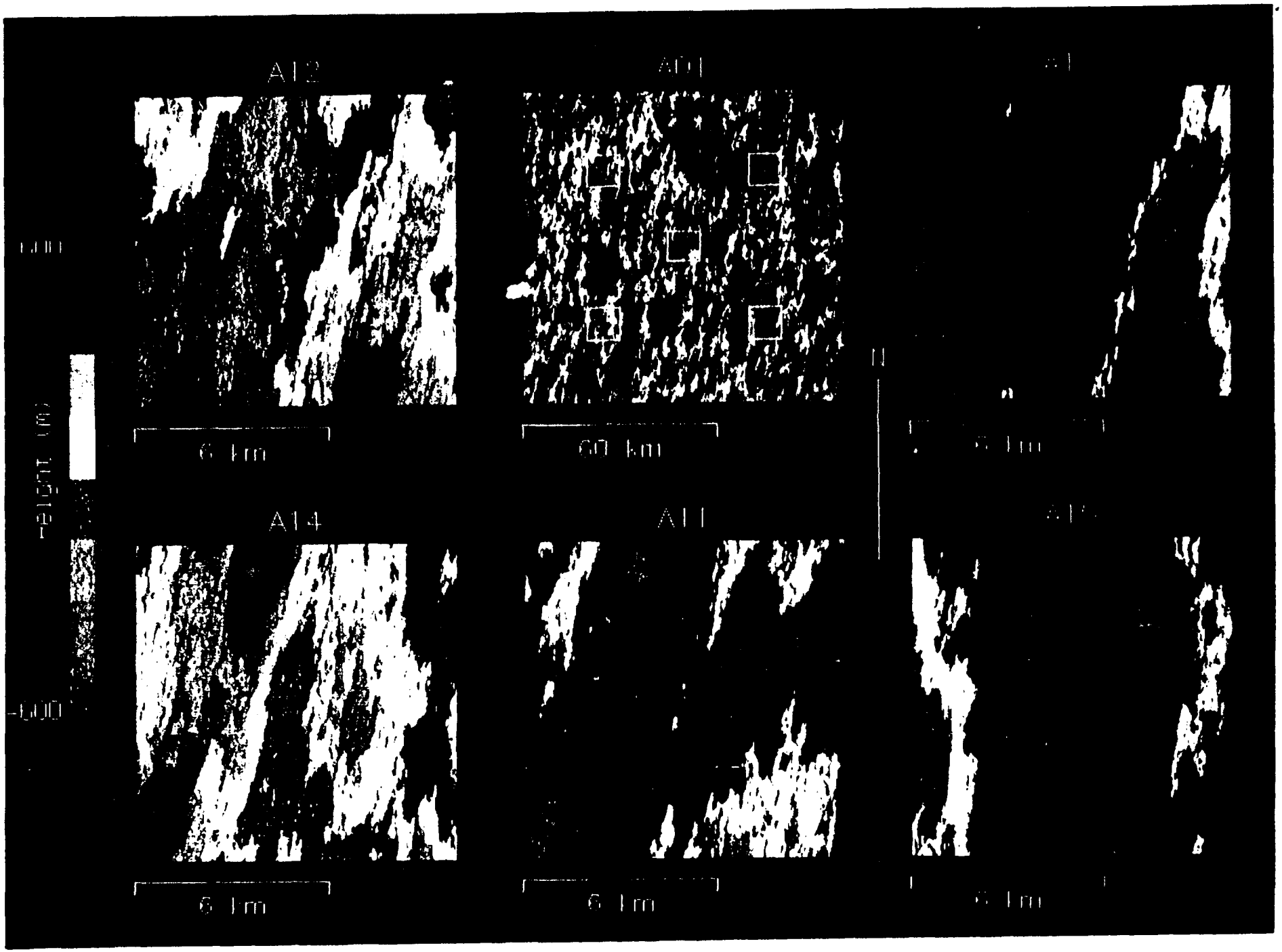

Figure 6

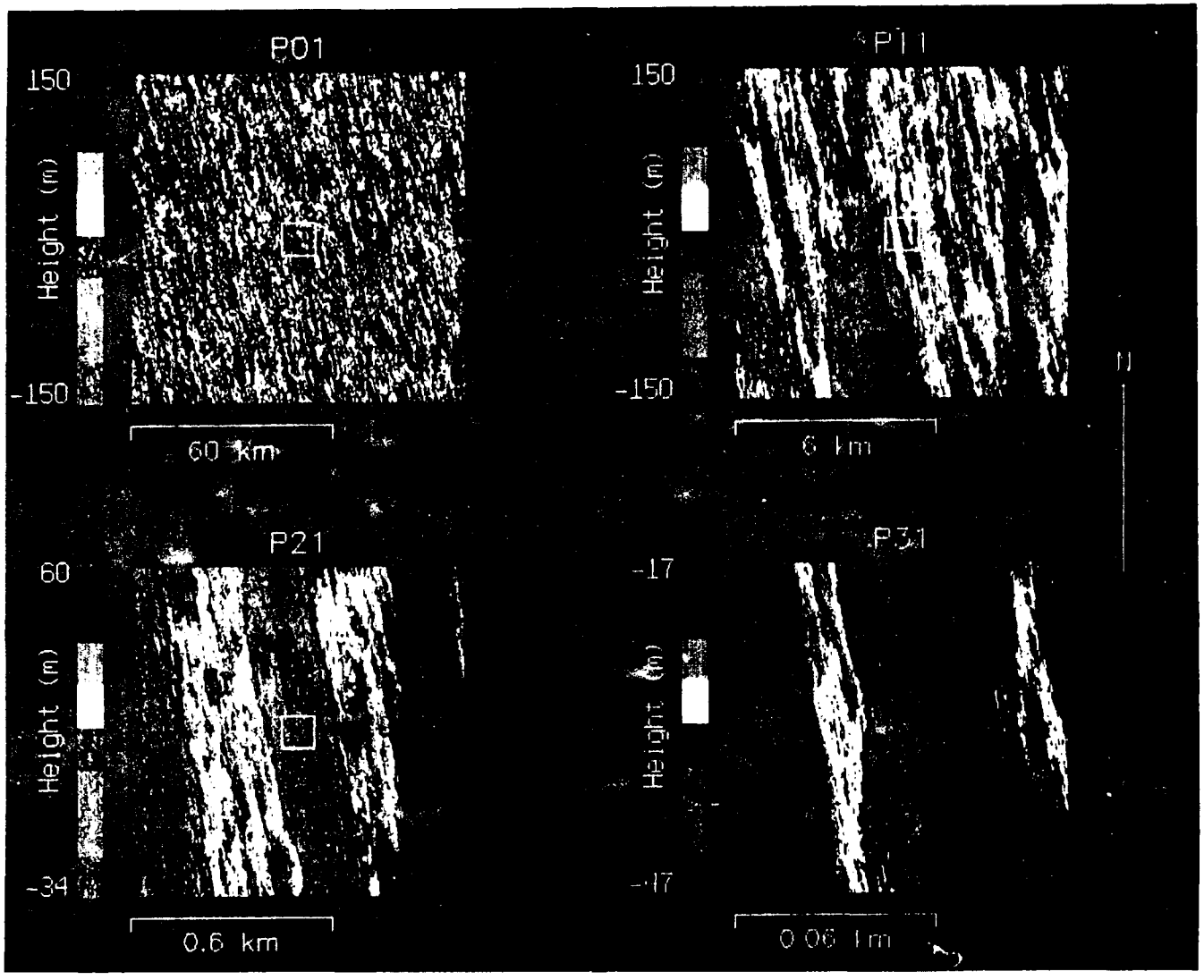
P01
150
Height (m)
-150
60 km
P11
150
Height (m)
-150
6 km
P21
60
Height (m)
-34
0.6 km
P31
-17
Height (m)
-17
0.06 km

Figure 7

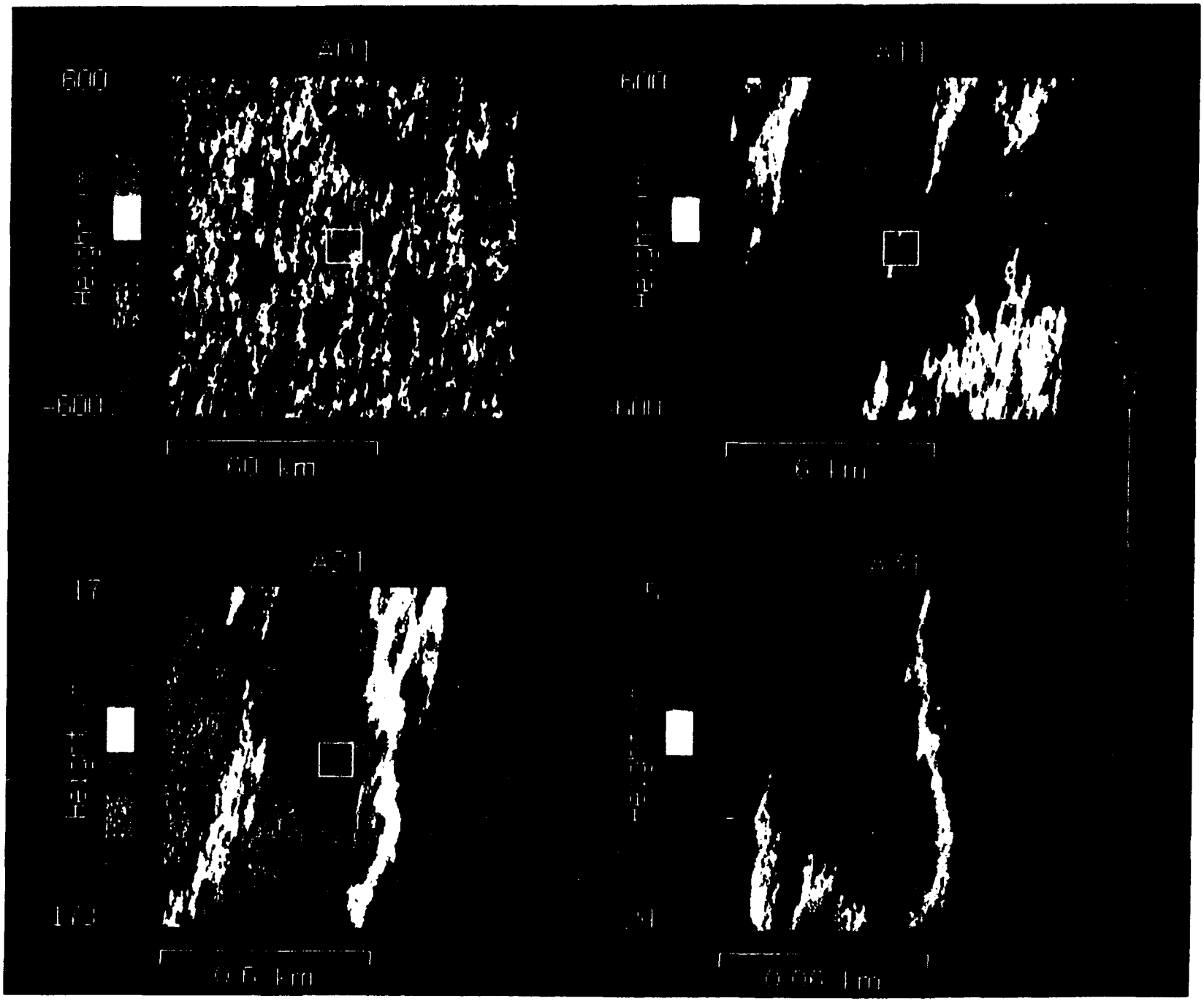

Figure 8